Journal of Colloid and Interface Science 653 (2024) 1432–1443

Contents lists available at ScienceDirect

Journal of Colloid And Interface Science

journal homepage: www.elsevier.com/locate/jcis

Surface forces and friction between Langmuir-Blodgett polymer layers in a nonpolar solvent

Nicholas M. Taylor [a,1], Georgia A. Pilkington [a,2], Tim Snow [a,3], Peter J. Dowding [b], Beatrice N. Cattoz [b], Andrew D. Schwarz [b,4], Oier Bikondoa [c,d], Brian Vincent [a], Wuge H. Briscoe [a,*]

[a] School of Chemistry, University of Bristol, Cantock's Close, Bristol BS8 1TS, UK
[b] Infineum UK Ltd, Milton Hill Business and Technology Centre, Abingdon, Oxon OX13 6BB, UK
[c] XMaS, The UK CRG Beamline, European Synchrotron Radiation Facility (ESRF), 71 Avenue des Martyrs, 38043 Grenoble, France
[d] Department of Physics, University of Warwick, Gibbet Hill Road, Coventry CV4 7AL, UK

GRAPHICAL ABSTRACT

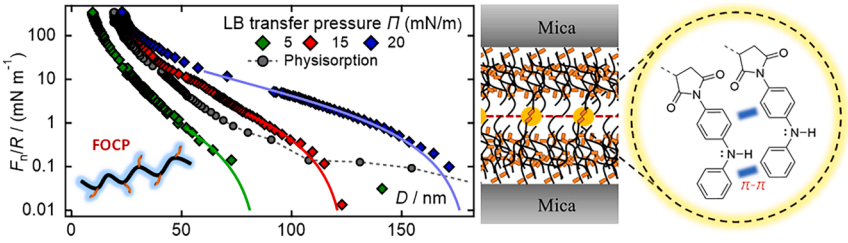

ABSTRACT

Optimization of boundary lubrication by tuning the confined molecular structures formed by surface-active additives such as surfactants and polymers is of key importance to improving energy efficiency in mechanical processes. Here, using the surface forces apparatus (SFA), we have directly measured the normal and shear forces between surface layers of a functionalised olefin copolymer (FOCP) in *n*-dodecane, deposited onto mica using the Langmuir-Blodgett (LB) technique. The FOCP has an olefin backbone decorated with a statistical distribution of polar-aromatic groups, with a structure that we term as "*centipede*". The effect of lateral confinement, characterised by the surface pressure, Π_{dep}, at the air–water interface at which the LB films are transferred, was examined. Normal force profiles revealed that the thickness of the LB films increased significantly with Π_{dep}, with the film thickness ($t > 20$ nm) inferring a multi-layered film structure, consistent with the interfacial characterisation results from synchrotron X-ray reflectivity (XRR) measurements. The coefficient of friction, μ, between the LB films spanned two orders of magnitude from superlubricity ($\mu \sim 0.002$) to much higher friction ($\mu > 0.1$) depending nonlinearly on Π_{dep}, with the lowest friction observed at the intermediate Π_{dep}. Molecular arrangement upon LB compression leads to the multilayer film with a structure akin to an interfacial gel, with transient crosslinking facilitated by the intra- and inter-molecular interactions between the functional groups. We attribute the differences in frictional behaviour to the different prevalence of the FOCP functional groups at the lubricating interface, which depends sensitively on the degree of compression at the air–water interface prior to the LB deposition. The LB films remain intact after repeated compression (up to pressures of 10 MPa) and shear cycles, indicating strong surface anchorage and structural robustness as a load-bearing and shear-mediating boundary layer. These unprecedented results from the friction measurements between LB films of a statistical copolymer in oil point towards new strategies for tailoring macromolecular architecture for mediating efficient energy dissipation in oil-based tribological applications.

* Corresponding author.
E-mail address: wuge.briscoe@bristol.ac.uk (W.H. Briscoe).
[1] Present address: Syngenta, Jealott's Hill International Research Centre, Bracknell RG42 6EY, UK.
[2] Present address: Division of Surface Chemistry and Corrosion Science, Department of Chemistry, KTH Royal Institute of Technology, 100 44 Stockholm, Sweden.
[3] Present address: Diamond Light Source, Harwell Science and Innovation Campus, Didcot, Oxfordshire OX11 0DE, UK.
[4] Present address: Fluorok Ltd, Begbroke Science Park, Oxfordshire, UK.

https://doi.org/10.1016/j.jcis.2023.09.146
Received 13 July 2023; Received in revised form 28 August 2023; Accepted 24 September 2023
Available online 26 September 2023

1. Introduction

Controlling friction and wear between contacting surfaces in relative motion is important to sustainability in a wide range of industrial and engineering scenarios, with immense economic, environmental, and societal impact. An estimated 20% of the world's energy consumption (equivalent to 103 EJ) [1] is spent overcoming friction within tribological contacts and, in an average passenger car, this accounts for a third of total fuel consumption [2]. The development of new lubrication strategies is therefore crucial to reducing friction and wear, improving energy efficiency, and reducing global emissions of CO_2 and other pollutants. It is also relevant to efficient and safe operation in future transportation (e.g. electrical vehicles) and off-shore energy generation (e.g. wind turbine bearings).

A key objective in oil-based tribology is friction reduction in the boundary and mixed lubrication regimes of the Stribeck curve [3], where the highest friction and wear typically occurs. Several classes of compounds known as friction modifier additives [4] are added to lubricant oils to reduce friction in the boundary regime, including oil-soluble surfactants commonly known as organic friction modifiers (OFMs) and organometallic compounds. Relatively recently, functionalised polymers traditionally used in other roles within the lubricant oil (e.g. as viscosity modifiers and dispersants) were also shown to form adsorbed boundary films that effectively reduced friction [5,6]. Several novel functionalised polymer chemistries have been designed to specifically act as polymer friction modifiers (PFMs) [7–13]. The common theme in these studies was the incorporation of both polar (anchor) and non-polar (buoy) [14] monomer blocks into the polymer structure, to combine strong physisorption to the polar surfaces with densely packed non-polar blocks extending out into the oil, facilitating an effective surface anchored boundary film between rubbing surfaces.

Fundamentally, these examples have all utilised polymer physisorption from solution to form the boundary lubricant layers. An alternative approach is to pre-deposit or synthetically grow polymer layers from surfaces, essentially acting as a surface treatment prior to their immersion in oil. Polymer brushes are a prime example of this strategy and have attracted strong interest as potential boundary lubricants due to the high polymer chain grafting densities that can be achieved, particularly when using grafting-from synthesis techniques such as atom-transfer radical polymerization (ATRP) [15,16]. Several examples exist of effective lubrication being provided by polymer brush layers in non-polar solvents, prepared by both grafting-to and grafting-from methods [17–20].

In several of these previous studies, comparisons between the lubrication efficacy of different PFMs (with a view to establishing a structure–activity relationship) focussed on the polymer chemical structure, such as the specific monomers used or the polymer molecular weight. However, there is also scope to explore physical methods to elicit changes in the interfacial structure, without modifying the polymer chemical structure through challenging synthesis routes. For an amphiphilic polymer, self-assembly can be facilitated at the air–water interface using a Langmuir-Blodgett (LB) trough [21], with the lateral polymer packing density in the interfacial layer readily tuneable by changing the trough surface area. Subsequent transfer of the polymer layer to a solid substrate (LB deposition) can produce densely packed LB films with the potential to provide friction reduction in the boundary regime, analogously to LB films formed by surfactants [22–24]. Only a few examples of frictional studies of polymer LB films can be found in the literature, all performed in air [25–27]. To the best of our knowledge, no frictional studies have ever been reported between polymer LB films immersed in a non-polar solvent. Additionally, none of these previous studies of polymer LB films investigated the effect of changing the packing density at the air–water interface prior to deposition, which is one of the key parameters probed in the current study.

Here, we have studied a statistical functionalised olefin copolymer (FOCP). This class of statistical copolymer has traditionally been used as dispersants and viscosity index improvers (VII) in lubricant oils [28], although their ability to reduce friction in the boundary regime is a relatively recent discovery. Surface layers of a centipede FOCP were LB-deposited on mica surfaces, with complementary characterisation of the dry-film interfacial structure on mica provided by X-ray reflectivity (XRR) [29–31]. The normal and shear forces acting between adjacent LB films in *n*-dodecane (acting as the model oil solvent) were measured using the surface forces apparatus (SFA) [32,33]. revealing a non-linear trend in the coefficient of friction (COF) as a function of the surface pressure, Π_{dep}, at which the LB films were deposited. Our results demonstrate the dramatic effect an intimate change in interfacial structure can have on the resulting lubrication behaviour and point towards new strategies for tuning boundary lubrication in oil using PFMs, with implications for the optimisation of lubrication in mechanical processes and resulting environmental and economic benefits.

2. Materials and methods

2.1. Materials

The functionalised olefin copolymer (FOCP, with the number and weight averaged molar weight $M_n = 59{,}004$ g mol^{-1} and $M_w = 107{,}908$ g mol^{-1}, respectively) consists of a hydrophobic poly(ethylene)-poly (propylene) (PE/PP) backbone bearing a statistical distribution of grafted N-(4-aminophenyl)aniline groups (functionalisation percentage ~ 6 wt%) (Fig. 1). The FOCP was synthesised by Infineum UK Ltd. using an established synthetic route where the aromatic amine is grafted onto the PE/PP backbone *via* a maleic anhydride linker [34], and was used as received without further purification. Anhydrous *n*-dodecane (≥99%, Honeywell) was either drawn directly from a freshly opened bottle or dried over activated molecular sieves (4 Å pore size) for 72 h prior to use. Ultrapure water (Milli-Q) was prepared using a Rios-5 – Milli-Q Gradient A10 system (Millipore). The water specific resistivity was 18.2 MΩ cm and the total concentration of dissolved organic compounds (TOC) was ≤ 3 ppb. Ruby muscovite mica (A1 Optical Grade) was purchased from S&J Trading, New York. Silver shot (Ag, ≥ 99.9999%) was purchased from Sigma Aldrich.

2.2. Langmuir-Blodgett (LB) deposition

FOCP layer preparation at the air–water interface was carried out using a KSV Nima KN 2002 Langmuir-Blodgett (LB) deposition trough, utilising water (Milli-Q) as the subphase and equipped with a platinum Wilhelmy plate for the measurement of surface pressure, Π [35], as shown in Fig. 2**a**. The trough was operated on an active anti-vibration table (Halcyonics GMBH, Germany) enclosed within a Perspex cabinet to minimise vibrations and prevent deposition of dust onto the water surface. For the preparation of X-ray reflectivity (XRR) samples, mica

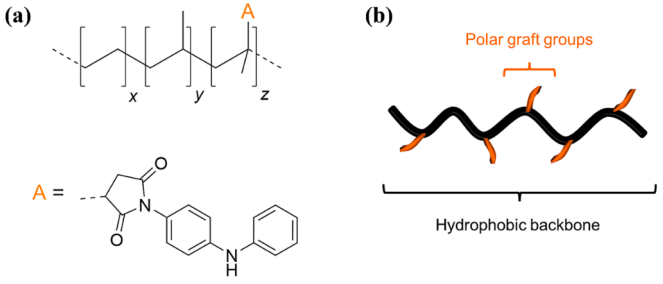

Fig. 1. (a) Molecular structure of the FOCP a hydrophobic poly(ethylene)-poly (propylene) (PE/PP) backbone bearing a statistical distribution of grafted N-(4-aminophenyl)aniline groups (functionalisation percentage ~ 6 wt%), with × ~ 1050–1920, *y* ~ 620–1135, and *z* ~ 13–24 and (b) Schematic representation of the 'centipede' architecture of the FOCP with the functional group (A in (a)) as the "legs".

substrates were hand-cleaved to 100–300 μm in thickness in a laminar flow hood (LFH) and cut to 1 × 3 cm in size with a pair of tailor's scissors, as required for use in 'bent mica' XRR measurements [31]. The freshly cleaved rectangular substrates were then gently secured to the dipper attachment of the LB trough using a Teflon crocodile clip and immersed in the water subphase prior to addition of the FOCP surface layer. For surface forces apparatus (SFA) measurements, the quartz lens-mounted mica surfaces were mounted into a custom-made dipper attachment based on the design of Tsarkova *et al.* [36] (Fig. 2**a**) and pre-immersed in the same way, with the apexes of both cylindrical lenses aligned perpendicular to the subphase.

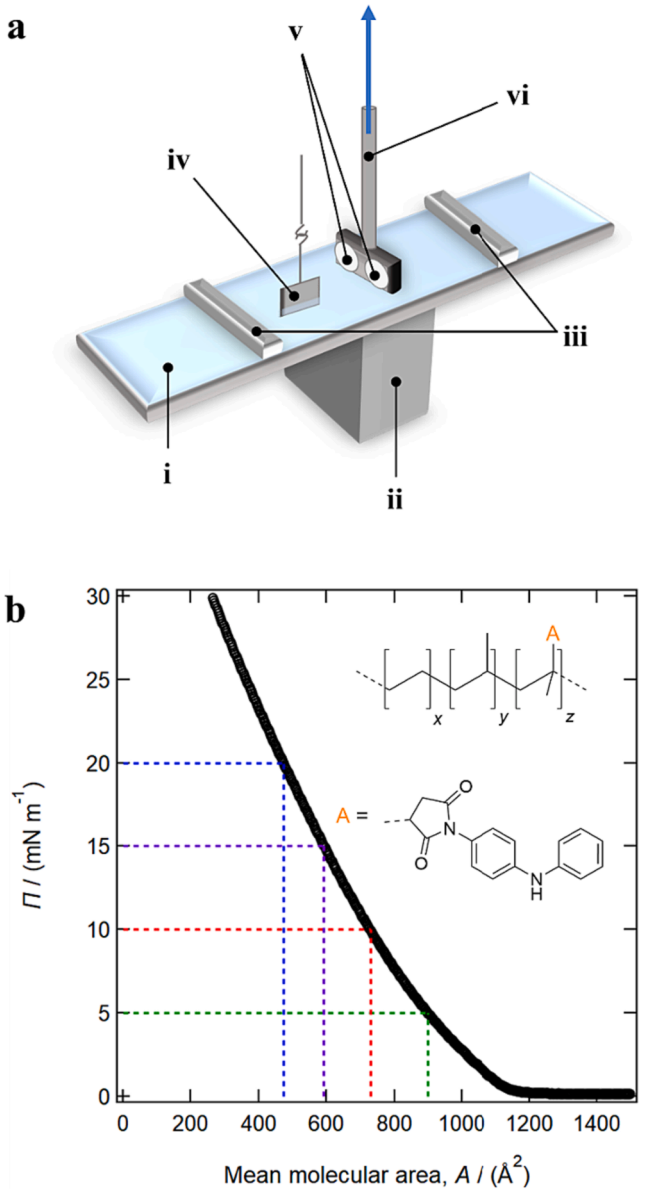

Fig. 2. (a) Schematic showing the process for Langmuir-Blodgett (LB) deposition of the FOCP simultaneously onto two mica surfaces used in SFA measurements. A solution of FOCP in chloroform ($CHCl_3$, 7.8 mg ml^{-1}, ~ 25 – 50 μl) is applied dropwise onto the water (Milli-Q) surface (i) prepared in a Langmuir trough equipped with a deposition well (ii) for the transfer of LB films to solid surfaces. The surface pressure, Π, of the FOCP film is controlled by a pair of barriers moving symmetrically (iii) and measured by a platinum Wilhelmy plate (iv). The mica surfaces, which are glued onto cylindrically curved quartz lenses (v), are secured onto a custom-made stainless steel dipper attachment (vi) [36]. The dipper is then immersed in the ultrapure water subphase prior to addition of the FOCP surface layer. (b) The surface area – pressure (Π-A) isotherm of the FOCP; the mean molecular area, A, is estimated from the number-average molecular weight, M_n, of the FOCP. The FOCP chemical structure is shown in the inset. The dashed lines show the four values of Π (5, 10, 15 and 20 mN m^{-1}) where LB deposition was performed.

After immersion of the substrates, a solution of the FOCP in chloroform ($CHCl_3$, 7.8 mg ml^{-1}, 25 – 50 μl). was applied dropwise to the surface of the water subphase. After 10 min solvent evaporation, the layer was compressed to the target value of Π at a constant barrier speed of 5 mm min^{-1}. The layer was then held at the target Π value for 30 min prior to its transfer *via* LB deposition to the solid (mica) substrates. LB deposition was carried out at four different surface pressures, Π_{dep} = 5, 10, 15 and 20 mN m^{-1} (Fig. 2**b**), and all the substrates were withdrawn from the subphase at a constant speed of 3 mm min^{-1}. The LB-film-coated surfaces were dried in a desiccator in the presence of phosphorus pentoxide (P_4O_{10}) for ~ 12–15 h prior to remounting in the SFA.

2.3. X-ray reflectivity (XRR)

XRR measurements were performed at beamline BM28 (XMaS) at the European Synchrotron Radiation Facility (ESRF), Grenoble, France. Measurements employed the 'bent mica' method [30,31] and the corresponding liquid cell described previously [31]. Briefly, the LB-film-coated rectangular mica substrates were bent over an underlying stainless steel cylindrical support of radius R = 7.5 cm and gently clamped in place by two stainless steel plates. This process rigidifies the mica substrate along the bending axis, providing sufficient flatness along this axis to carry out XRR measurements. The X-ray beam energy was 14 keV (with a corresponding wavelength λ = 0.89 Å) and the beam size was 400 μm (vertical FWHM) × 254 μm (horizontal FWHM). After sample alignment, the specularly reflected beam intensity at each angle $\theta_r = \theta_i$ was collected using an avalanche photodiode detector (APD). Data points were collected with an integration time of 1 – 2 s at each angle, over an incident angle range of θ_i = 0.06 – 2.60°, corresponding to a momentum transfer vector perpendicular to the surface, Q_z, range of 0.015 – 0.64 $Å^{-1}$, where $Q_z = (4\pi\sin\theta_i)/\lambda$.

The data were normalised and corrected to account for both the sample width (9 – 10 mm) and the Gaussian intensity profile of the beam (derived from a spline fit to a fine height scan of the sample at an incident angle θ_i = 0°). Analysis of XRR data on mica must consider the contribution of the mica crystal truncation rods (CTR) to the overall reflectivity; the first mica CTR peak occurs at $Q_z \approx 0.63$ $Å^{-1}$, which is within the typical Q_z range where the Kiessig fringes from the sample are seen. The XRR data were fitted using a Python software package employing the standard Parratt algorithm [37] and incorporating a 'dual layer' approximation to account for the first CTR of the mica substrate as described in detail previously [31]. The mica unit cell is modelled as two layers whose relative thickness and scattering length density (SLD) are allowed to vary, with constraints applied to ensure that the overall unit cell thickness (t = 9.94 Å) and the bulk SLD of mica are conserved. A total of 450 of these bilayers are used to model the underlying mica substrate. The overlying sample is then divided into a finite number of homogeneous layers or slabs. Each layer is characterised by its own distinct thickness, t, roughness, σ, and SLD, ρ. These three parameters are varied for each layer and the computed reflectivity compared with the experimental data points until an optimal fit is achieved.

2.4. Surface forces apparatus (SFA)

The SFA has been described in detail previously [32,38] and its key elements are shown schematically in Fig. 3. The normal (F_n) and shear (F_s) forces between two back-silvered mica surfaces (2–7 μm in thickness) are measured *via* the deflection of two orthogonal sets of springs, respectively. The surface separation, D, at the point of closest approach between the two surfaces is determined using multiple-beam interferometry. D can be measured to ± 2–3 Å through monitoring the wavelengths of the resulting fringes of equal chromatic order (FECO) [39],

which allows determination of the deflection of the horizontal leaf springs for measurements of F_n. Normal force profiles, F_n/R, as a function of D were recorded for both approach (compression) and separation (decompression) of the two surfaces. F_n/R is the normal force normalised by the radius of curvature of the two approaching surfaces; as derived in the Derjaguin approximation [40] this is proportional to the interaction energy per unit area between two flat surfaces, allowing comparison of results obtained between surfaces of different curvatures.

The SFA used in these experiments [32] has the shear measurement capability originally designed by Klein, who often refers to this version of the instrument as the surface force balance (SFB) [38]. Lateral shear motion is applied to the top surface by a sectored piezoelectric cylinder on which the top surface is mounted; the bending of the vertical springs, Δx, in response to an applied shear force, is monitored by an air–gap capacitance probe, allowing determination of F_s. Digital signal control is managed using a field-programmable gate array (FPGA) and data acquisition is controlled by a custom-designed LabVIEW interface programme, as described previously [32].

Mica sheets were hand-cleaved to a thickness of 2 – 7 μm in a laminar flow hood (LFH) and immediately adhered to a freshly cleaved mica backing sheet to prevent particulate contamination. A thin layer of silver (~40 – 50 nm) was deposited onto the mica by resistive evaporation at a pressure of ~ 10^{-6} torr using either an Edwards E306 coating system or a Korvus HEX series thin film evaporation system. The back-silvered mica pieces were glued onto cylindrically curved quartz discs (R ~ 1 cm) using Epon 1004 (Shell) and mounted in a crossed cylinders geometry inside the apparatus.

All the SFA measurements were carried out in the presence of P_4O_{10}, to maintain a dry atmosphere inside the chamber. After calibration of the mica-mica contact in air, the mica surfaces were either removed for Langmuir-Blodgett deposition or left in place prior to solution injection between the two surfaces. For the physisorption experiment, approximately 18 ml of FOCP solution in *n*-dodecane (concentration c_{pol} = 0.5 wt%) was injected between the mica surfaces and was left for ~ 3 hr before normal and shear force measurements were conducted between the resulting adsorbed layers. For the LB films, the dried surfaces were remounted in the SFA as close to their original orientation as possible and the normal and shear force measurements were performed in air and subsequently when immersed in pure *n*-dodecane. The forces curves presented below are representative of the results from 24 different contact positions from 8 different SFA experiments.

3. Results and discussion

3.1. XRR characterisation of FOCP LB films

XRR measurements revealed the interfacial structure of the FOCP LB films in air, transferred to mica at different surface pressures, Π_{dep}. The XRR curves at Π_{dep} = 5, 10 and 15 mN m^{-1} (Fig. 4) exhibit clear intensity oscillations (i.e. Kiessig fringes) [41], from the deposited polymer layers at $Q_z < 0.3$ $Å^{-1}$. The data were fitted using a one-layer slab model (Fig. 4 inset; fit parameters listed in Table 1) treating the polymer film as a homogeneous slab of uniform SLD, ρ.

The thickness t of the FOCP LB films increased significantly as a

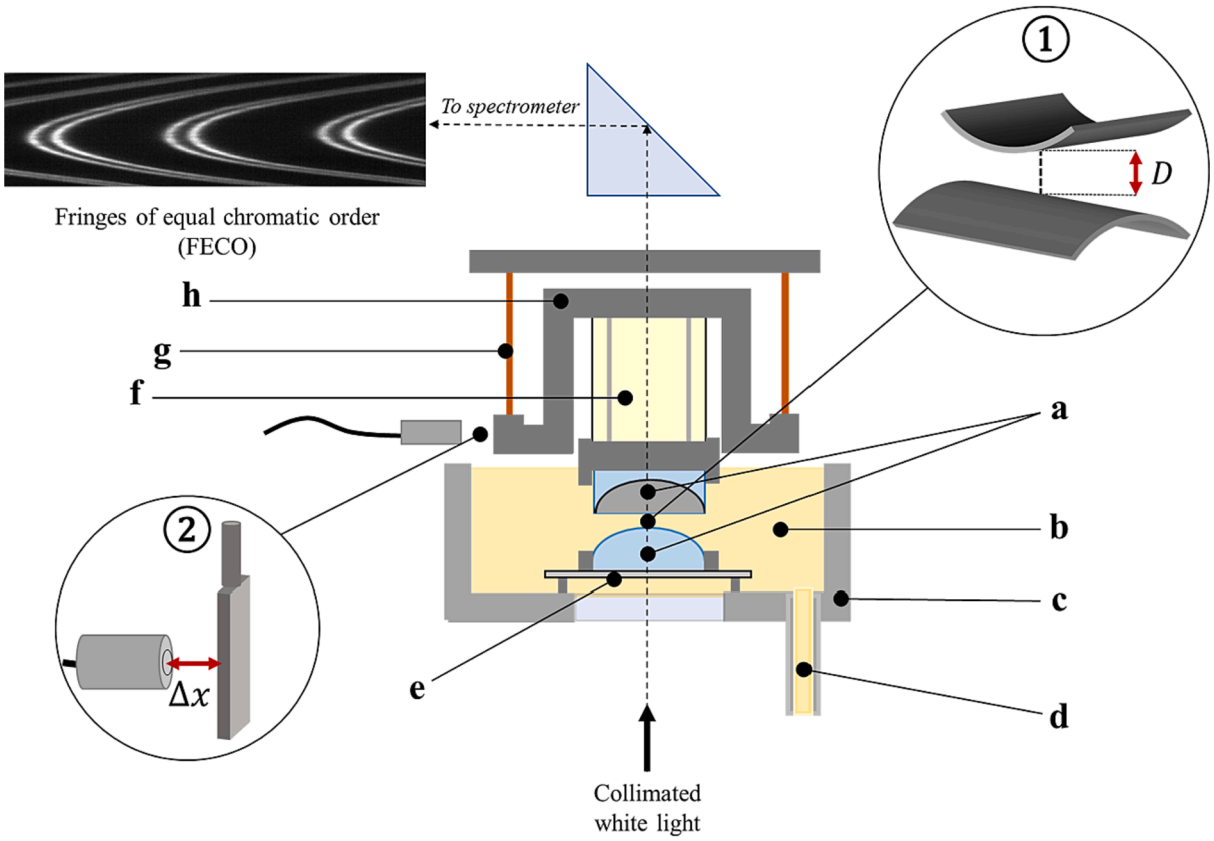

Fig. 3. Schematic showing the set-up of the SFA. Two back-silvered mica surfaces are glued to cylindrically curved quartz lenses (**a**, R ~ 1 cm) and are mounted in a crossed-cylinder geometry ($\theta = 90°$) as shown in inset ①. Collimated white light is directed normal to the contact area and the closest surface separation, D, between the surfaces is determined from the fringes of equal chromatic order (FECO) generated by the optical cavity (mica-sample-mica) present between the two silver layers. The surfaces can be immersed in a liquid medium (**b**) injected into a stainless-steel boat (**c**) *via* a system of PTFE tubing (**d**). The normal force, F_n, acting between the surfaces is measured from the deflection of the horizontal leaf springs (**e**) on which the lower surface is suspended. Lateral shear motion is applied to the upper surface by a hollow, sectored piezoelectric cylinder (**f**), which is coupled to a second set of vertical springs (**g**) by a rigid bridge (**h**). The deflection of the vertical springs, Δx, is measured by an air–gap capacitance probe (inset ②) and used to calculate the shear force, F_s.

function of Π_{dep}, from $t = 22.2$ nm at $\Pi_{dep} = 5$ mN m^{-1} to $t = 34.8$ nm at $\Pi_{dep} = 15$ mN m^{-1}. The formation of monolayers at the air–water interface by different statistical copolymer chemistries has been demonstrated in the literature, with typical film thicknesses of $t < 5$ nm reported [42,43]. By comparison, the values of t (>20 nm) obtained for the FOCP LB films are much higher and increased significantly with Π_{dep}, which strongly supports the presence of multiple FOCP layers (i.e. not a monolayer) within the LB films. From fitting, the roughness, σ, of the FOCP LB films was significant ($\sigma > 0.5$ nm) and increased with Π_{dep}, from $\sigma = 0.6$ nm at $\Pi_{dep} = 5$ mN m^{-1} to $\sigma = 1.0$ nm at $\Pi_{dep} = 15$ mN m^{-1}, which is consistent with the more rapid decay in Kiessig fringe amplitude at higher Π_{dep}. XRR data were also obtained for LB films deposited at $\Pi_{dep} = 20$ mN m^{-1} but could not be successfully fitted as Kiessig fringes were absent from the data, likely due to a complete dampening in fringe amplitude caused by a further increase in σ. The calculated SLDs ($\rho = 2.84 - 3.43 \times 10^{-6}$ Å^{-2}) were lower than the theoretically calculated SLD of the pure FOCP ($\rho = 8.36 \times 10^{-6}$ Å^{-2}), leading to an estimated average surface coverage range of 34 – 41%.

Across all the SFA measurements (see below) performed between the LB films in air and *n*-dodecane, only small differences in the surface layer thickness were observed at different contact positions, inferring a rather homogeneous surface coverage. The typical contact area in the SFA measurements (<700 μm^2) is much smaller than the X-ray beam footprint (~1 cm × 250 μm = 250,000 μm^2) on the surface during XRR measurements and so the SFA probes more localized surface structure. It is conceivable that the film had a relatively open 3D network, akin to an interfacial gel, instead of a highly heterogenous surface distribution of islands of polymers.

We also note that the XRR fit parameters are obtained from a simple one-slab model (Fig. 4 inset), and it thus does not account for a more heterogeneous SLD profile normal to the interface. For instance, the presence of a thinner underlayer of FOCP with a sufficiently high roughness would not have been distinguishable by XRR measurements.

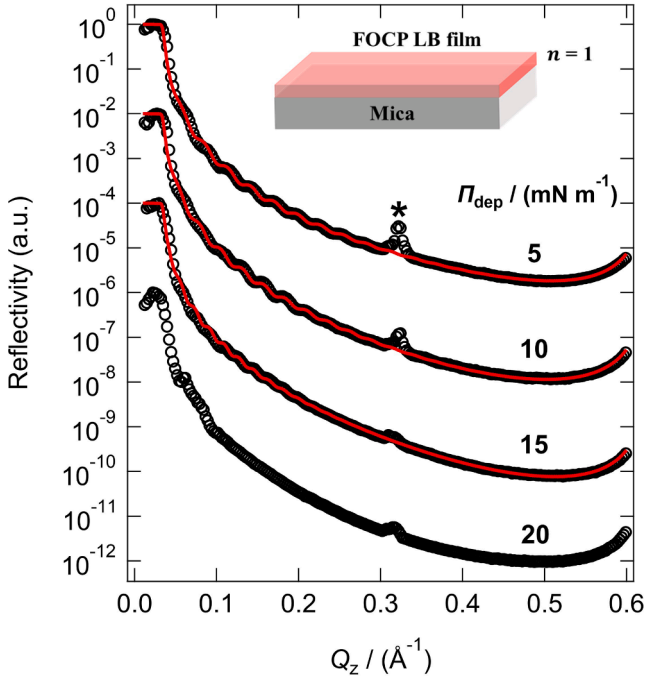

Fig. 4. XRR curves (R vs Q_z) obtained for the FOCP LB films in air, deposited onto mica at four different values of surface pressure, Π_{dep}. The solid red lines are fits to a one-layer slab model (inset). The asterisk denotes the position of the 'forbidden' half-Bragg peak of mica ($Q_z \sim 0.32$ Å^{-1}), whose presence is not accounted for in the data-fitting procedure described here. The data for $\Pi_{dep} =$ 10, 15 and 20 mN m^{-1} are vertically offset for clarity by factors of 10^{-2}, $10^{-4}$and 10^{-6}, respectively.

Table 1
Fitting parameters corresponding to the XRR data shown in Fig. 4. Also listed is the apparent mean molecular area, A obtained from the Π-A isotherm (Fig. 2**b**), $D_0/2$ (i.e. half of the adhesive contact separation) obtained from the SFA measurements in air, and D_{sd} (defined in the main text).

Π_{dep} / (mN m^{-1})	A / (Å^2)	t (XRR)/ nm	ρ / 10^{-6} Å^{-2}	σ / nm	$D_0/2$ / nm (SFA)	D_{sd} / nm (SFA)
5	899	22.2	2.84	0.6	8.7 (±2.7)	43.4
10	729	24.1	3.34	0.7	18.1 (±4.0)	54.2
15	592	34.8	3.43	1.0	17.0 (±1.5)	75.1
20	473	–	–	–	34.8 (±0.3)	51.1

However, these limitations do not detract from the main qualitative trend: that is, an increase in Π_{dep} led to an increase in the thickness and roughness of the resulting FOCP LB nanofilms likely with a gel-like structure, which is consistent with SFA normal force measurements. Owing to the poor SLD contrast between the FOCPs and *n*-dodecane ($\rho = 7.33 \times 10^{-6}$ Å^{-2}), complementary XRR measurements at the buried mica-oil interface were not possible, thus limiting the use of XRR to the mica-air interface in this work. This could be remedied in future by employing neutron reflectivity (NR), where selective deuteration of different components of the system would generate sufficient SLD contrast to perform such measurements.

3.2. Normal forces between the LB films

In air, the surfaces bearing the LB films experienced no detectable interactions (cf. **Fig. S2** in Supplementary Information (SI) section) until they came to close proximity of each other, from which the attractive van der Waals force caused the two opposing LB films to spontaneously "jump" into an adhesive contact at the surface separation of $D_0 = 17.3$, 36.1, 34.0 and 69.5 nm for $\Pi_{dep} = 5$, 10, and 15 and 20 mN m^{-1}, respectively, indicating an increasing dry film thickness of $D_0/2 = 8.7$ –34.8 nm (cf. Table 1) for a single LB film in each case, consistent with the trend seen in the XRR results presented above, although the XRR film thickness t was higher. This discrepancy could be attributed to the fact that the surface polymer layers would become compacted under the adhesive contact in the SFA measurements.

Fig. 5**a** shows representative normal force profiles between the two surfaces on approach obtained after immersion of the FOCP LB films in *n*-dodecane at all the Π_{dep} values, while Fig. 5**b** plots the data both on approach and separation of the surfaces at $\Pi_{dep} = 5$ and 20 mN m^{-1}. Upon approach of the two surfaces in dodecane, a monotonic repulsive interaction was observed for all four LB film conditions and between physisorbed FOCP layers. This behaviour is in stark contrast to the expected behaviour for confinement of the pure *n*-dodecane solvent, which shows no long-range interactions but exhibits an oscillatory structural force profile from its ordering into quasi-discrete layers at very small separations ($D < 5$ nm) [44,45]. The long-range repulsion observed thus confirms the presence of the FOCP surface layers.

From fitting the normal force profiles at larger D to the Alexander – de Gennes theory (solid lines in Fig. 5**a**, details given in the SI), the surface separation at which the FOCP LB films first came into repulsive contact can be estimated from the fitted value of L_0 (the unperturbed thickness of a single polymer layer, Fig. 5**a** legend) using $D = 2L_0$. The polymer layer thickness $L_0 = D/2$ in the range of ~ 43 – 91 nm is larger than that in dry air obtained from SFA and XRR (cf. Table 1), indicating that the polymer films were swollen with entrained *n*-dodecane solvent.

Similarly, D_{min}, (the "hard-wall" thickness, i.e. the smallest surface separation reached under high compression, cf. Fig. 5**b** and **Fig. S2 (SI)**) increased as a function of Π_{dep}, from $D_{min} \sim 9$ nm at $\Pi_{dep} = 5$ mN m^{-1} to

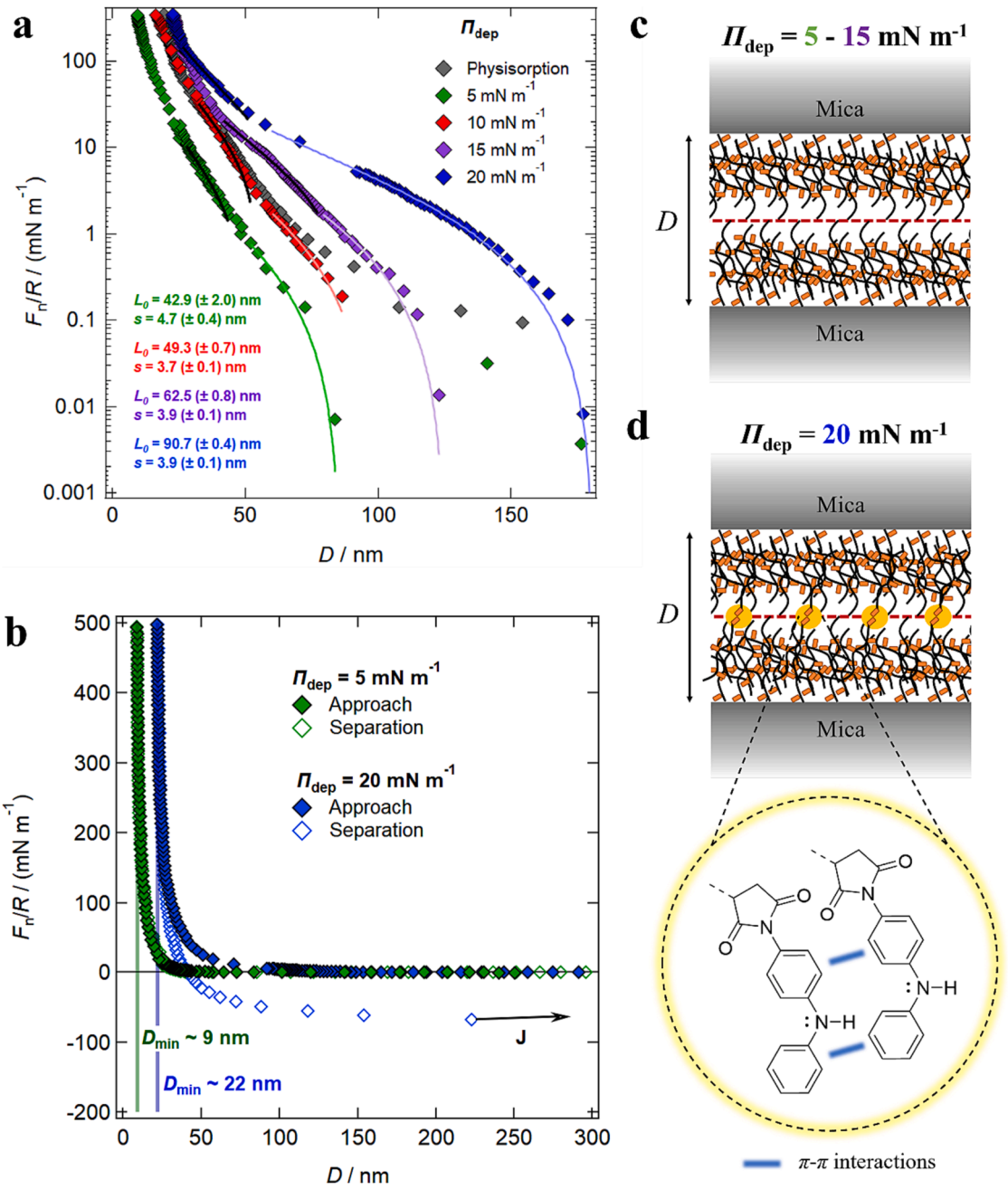

Fig. 5. Representative normal interactions, F_n/R, between the FOCP-coated mica surfaces (radius of curvature, $R \sim 1$ cm) in *n*-dodecane, as a function of the surface separation, D, and Π_{dep}. (a) Approach curves plotted on a semi-log scale, including data recorded between physisorbed FOCP layers ($c_{pol} = 0.5$ wt%). The coloured solid lines are fits to the lower part of the F_n/R vs. D profiles using the Alexander-de Gennes theory for neutral brush interactions (details in **SI**) and the corresponding values of unperturbed chain length, L_0, and inter-anchor spacing, s, are shown in the legend. The black lines are fits to the intermediate part of the F_n/R vs. D profiles using the functional form $F_n/R = (A/D^2) + B$ (where A and B are constants), consistent with the monomer concentration falling into the concentrated regime as discussed in the main text. (b) Approach and separation profiles at $\Pi_{dep} = 5$ and 20 mN m^{-1}, highlighting the attractive force upon separation for the latter and the corresponding jump-out of contact **J**. (c) Schematic showing the possible confined structure giving rise to the normal force profiles at $\Pi_{dep} = 5$, 10 and 15 mN m^{-1}. (d) Schematic showing the possible confined structure giving rise to the normal force profiles at $\Pi_{dep} = 20$ mN m^{-1}, with the postulated FG-FG interactions highlighted.

$D_{min} \sim 22$ nm at $\Pi_{dep} = 20$ mN m^{-1}. The thickness of a single layer, $D_{min}/2$ is ~ 4.5, 7.5 and 9.5 nm at 5, 10 and 15 mN m^{-1}, respectively, which is much smaller than the fitted thickness of a single layer in air obtained from XRR and smaller than $D_0/2$ in air (cf. Table 1). This indicates the network structure in the polymer nanofilm, akin to an interfacial gel (instead of an LB monolayer). Assuming that the $D_{min}/2$ value corresponds to a heavily compacted polymer layer, the calculated ratio of the two values, $(D_{min}/2)/t_{XRR}$ is 0.20, 0.31 and 0.27 at 5, 10 and 15 mN m^{-1}, respectively, which is the lower bound of the polymer volume fractions and not dissimilar to the polymer layer volume fractions estimated from the fitted SLD values in air (0.34, 0.40 and 0.41). This finding supports the hypothesis that the LB films consist of an open 3D network of FOCP chains with a significant amount of free space.

The Alexander – de Gennes fit to the SFA data also yields the effective blob size, $s \sim 3.7 – 4.7$ nm. Although the LB polymer gel layer is not a classic polymer brush (i.e. densely packed end-anchored polymer chains), its networked structural features bear resemblance to that of a polymer brush, at least under the low compression at larger D. Repeated

normal force profiles obtained after several cycles of compression and shear measurements were similar to those recorded upon first approach at the same contact area for all values of Π_{dep}, showing strong anchorage and robustness of the LB films on the mica surfaces and good durability towards shear-off under the conditions probed in this study.

At higher compression (i.e. higher F_n/R and lower D), the measured normal force profiles deviate significantly from the Alexander – de Gennes theory. The surface separation, D_{sd}, at which this deviation is observed depends on Π_{dep}, and thus on the polymer layer thickness, as also listed in Table 1. We may rationalise this discrepancy between the experimental force profiles and the theoretical prediction as follows. The Alexander – de Gennes theory has been devised for the semi-dilute regime (monomer volume fraction $\phi < \sim$10%) which predicts that the osmotic pressure due to monomer crowding scales with ϕ^2 (in the mean field approach) or $\phi^{9/4}$ (in the scaling approach) [46]. At higher compression and lower D, the monomer concentration exceeds this limit and the interactions in the concentrated regime are dominated by the osmotic pressure, scaling as ϕ^3 to the first approximation in Flory-Huggins theory [47]. It follows from the Derjaguin approximation that the interaction energy per unit area and thus F_n/R can be obtained by integrating the osmotic pressure over D; thus $F_n/R \sim \phi^2 \sim D^{-2}$. The solid black lines in Fig. 5**a** show the D^{-2} decay which indeed could describe the trend of the experimental F_n/R profile at the lower D much better.

The normal force profiles obtained between physisorbed layers of the FOCP (grey diamonds in Fig. 5**a**) were qualitatively different to those between the FOCP LB films. For example, comparing with the data at $\Pi_{dep} = 10$ mN m^{-1} (red diamonds in Fig. 5**a**), the normal force profiles were similar at higher compression (low D), but the characteristic Alexander – de Gennes shape was not observed at higher D and an earlier onset of repulsion ($D \sim 155$ nm) was seen. Unlike the case of the (pre-deposited) LB films, there is a reservoir of the FOCP in solution, leading to the formation of FOCP aggregates in the bulk solution. Our preliminary small-angle neutron scattering (SANS) measurements have confirmed the presence of FOCP aggregates at the bulk solution concentration ($c_{pol} = 0.5$ wt%) measured using the SFA. Furthermore, our complementary solution depletion adsorption isotherm measurements at the unperturbed single mica-dodecane interface suggest that FOCP adsorption is not limited to a monolayer, but instead further adsorption of multilayers and/or aggregates occurs as the bulk solution concentration is increased (manuscript in preparation). To verify this for the confined interfaces, we performed an additional SFA experiment where the FOCP was 'pre-adsorbed' from *n*-dodecane at the same concentration and measurements were performed between the adsorbed layers in pure *n*-dodecane (i.e. no polymer reservoir in solution) after the removal of weakly- and non-adsorbed FOCP by rinsing with the solvent (Supplementary Information, **Fig. S4**). This revealed a significant increase in the confined layer thickness in the FOCP-containing solution compared to pure *n*-dodecane, indicating further adsorption of polymer chains and their incorporation into the confined layer.

The presence of aggregates between the physisorbed FOCP layers present on both surfaces (trapped by the gradual confinement and/or weakly adsorbed) and their gradual expulsion under the compression applied in the SFA measurements could provide a plausible explanation for the longer-ranged repulsive force seen at higher values of D in the physisorption experiments. Additionally, the physisorbed FOCPs would have the non-adsorbed segments extending into the oil, contributing to a longer-range repulsion than that between the LB films; whilst the LB-deposited layer would be more compact (being in air upon the LB-transfer) prior to their immersion in *n*-dodecane. Despite the similarity between the normal force profiles at lower D, drastically different frictional behaviour was seen in the shear force measurements, reflecting subtle differences between the FOCP interfacial structures formed by physisorption and LB deposition respectively, as will be discussed in the shear forces section.

Upon separation of the surfaces, no attraction was observed for the LB films at $\Pi_{dep} = 5$, 10 and 15 mN m^{-1}. In contrast, for the LB films at $\Pi_{dep} = 20$ mN m^{-1}, an attractive force was observed prior to the surfaces jumping out of contact (**J** in Fig. 5**b**), indicating the presence of bridging interactions between the FOCP layers. As *n*-dodecane acts as a good solvent for the PE and PP monomers that account for the most of the constituent monomer units within each FOCP chain, the bridging interaction is attributed to attractive interactions between exposed solvophobic polymer functional groups (FGs), i.e. the grafted N-(4-aminophenyl)aniline groups, on the opposing FOCP layers (cf. Fig. 5**d**). Association of aromatic-functionalized olefin copolymers in non-polar media has been shown previously to be driven primarily by polar interactions between the succinimide groups when labelled with pyrene moieties [34,48]. Based on the chemical structure of the FOCPs described in this work, the FG-FG interactions are likely to arise from a combination of these polar interactions and π-π interactions between the aromatic rings, providing the driving force for FOCP association in the bulk *n*-dodecane solution and at the confined interfaces.

3.3. Shear forces between the LB films

Shear force measurements were also made as the LB films were progressively compressed and decompressed (i.e. as the surface separation D was decreased and increased) in *n*-dodecane. Fig. 6**a** shows the shear trace with a saw-tooth form, thus at a constant shear velocity, v_s between the two extremes of the shear trace, applied to the top surface as a function of time. An example of the corresponding shear response is also shown in Fig. 6**a**, where the displacement from the midpoint to the plateau is used to calculate the shear force, F_s, transmitted across the FOCP LB films. Plots of F_s against F_n obtained for all four values of Π_{dep} are shown in Fig. 6**c**. The data obtained between FOCP surface layers formed by physisorption from solution in *n*-dodecane ($c_{pol} = 0.5$ wt%) are also shown for comparison.

The coefficient of friction, μ, determined from the gradient of the F_s – F_n plots (Fig. 6**c**) varied significantly between the different Π_{dep} used for FOCP LB film deposition. A value of $\mu \approx 0.07$ was obtained between adsorbed FOCP layers formed by physisorption from 0.5 wt% FOCP solution in *n*-dodecane. By comparison, the μ value in pure *n*-alkane solvents is typically much higher ($\mu > 0.5$), for e.g. *n*-octane, *n*-tetradecane and *n*-hexadecane in comparable measurements performed between mica surfaces in an SFA [49,50]. This behaviour is attributed to the layering of *n*-alkane molecules under confinement and resulting solid-like response to shear [38], with the reported COFs occurring at typical surface separations of $D < 3$ nm (corresponding to fewer than six layers of confined alkane molecules) and normal loads $F_n/R < 10$ mN m^{-1}.

The FOCP LB films, LB transferred from the air–water interface to mica before immersion in *n*-dodecane, produced markedly different lubrication to the FOCP films physisorbed from *n*-dodecane, and μ varied dramatically as a function of Π_{dep}. At the lowest surface pressure, $\Pi_{dep} = 5$ mN m^{-1}, a value of $\mu = 0.03 – 0.04$ was obtained, representing a reduction in μ by a factor of ~ 2 relative to the physisorbed films. This is already quite a striking result, as the change in layer preparation process to LB deposition resulted in quite different friction reduction efficacy of the same FOCP.

At $\Pi_{dep} = 10$ mN m^{-1}, a surprisingly low value of $\mu = 0.002–0.003$ was seen at normal loads up to $F_n = 1000 – 4000$ μN (dependent on the shear velocity, v_s, used for the measurement), thus exhibiting superlubricity, a phenomenon defined arbitrarily by a COF of $\mu \leq 0.01$. The corresponding pressure lies in the range of $p \sim 30 – 48$ atm, as estimated from the Hertzian contact mechanics, i.e. $p = F_n/A = F_n/\left(\pi(F_nR/K)^{\frac{2}{3}}\right)$ [51] with $K \sim 9.5 \times 10^9$ Pa the approximate materials modulus for the mica-glue combination [33]. The LB films were intact under such high pressure and indeed after repeated shear (typically 10–15 normal and 5 shear force runs), evident from the reproducibility of the force curves and the lack of hysteresis upon compression and decompression. Interestingly, the measured COF of $\mu = 0.002–0.003$ is comparable to those

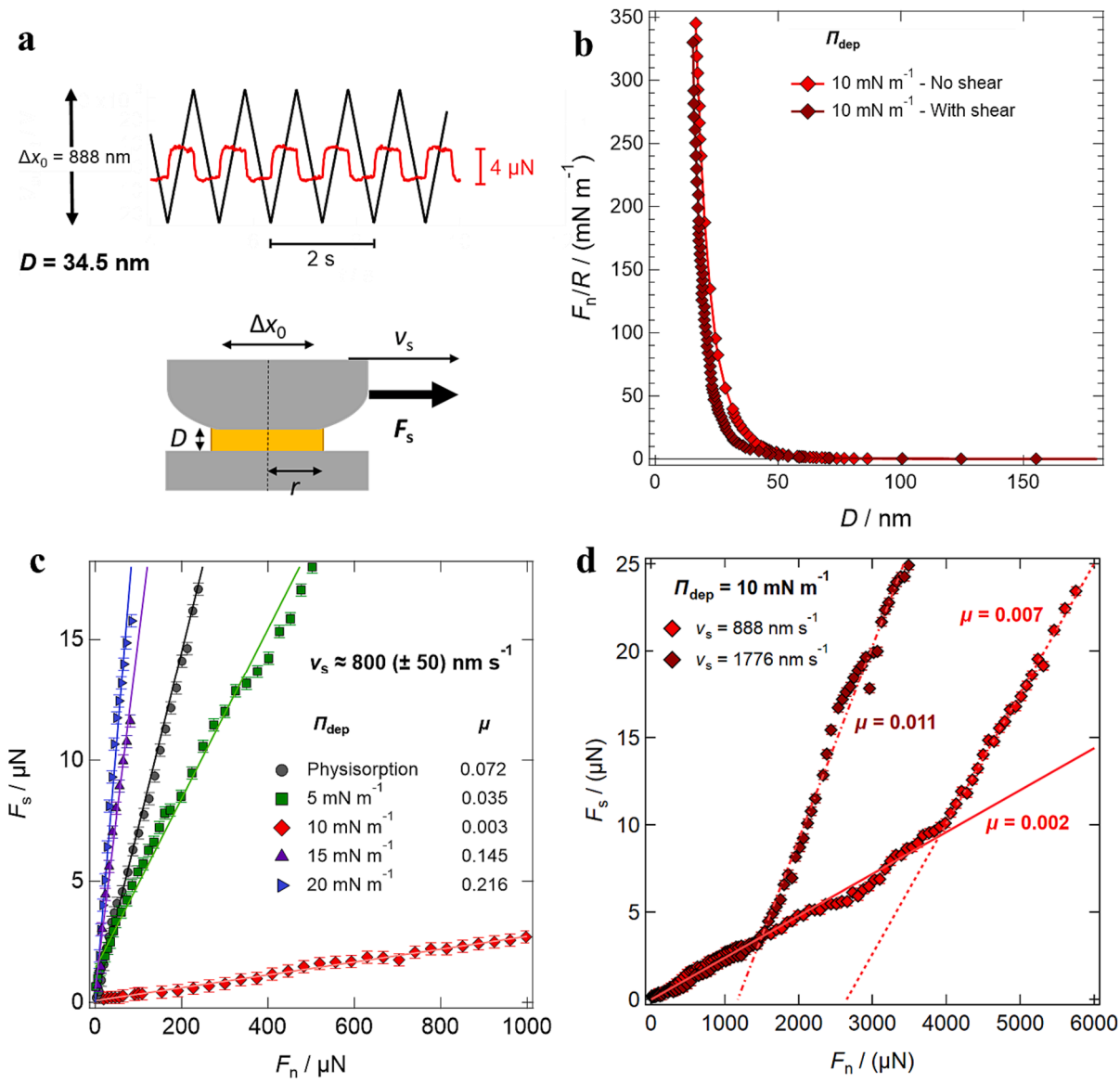

Fig. 6. SFA shear force results between two FOCP LB-films in *n*-dodecane. (a) The back-and-forth saw-tooth shear motion with a shear amplitude, Δx_0, applied to the top surface as a function of time (black trace) and an example (red trace) of the corresponding shear force, F_s, transmitted across FOCP LB layers at Π_{dep} = 10 mN m^{-1}, with an illustration of the configuration of the two cylindrically curved mica surfaces during shear. (b) Normal force profiles upon approach at Π_{dep} = 10 mN m^{-1}, both with and without shearing applied (c) Shear force, F_s, plotted against normal load, F_n, for all five deposition Π_{dep} conditions. The solid lines are linear fits to the data; the corresponding coefficients of friction, μ, are shown in the legend. (d) Shear force, F_s, plotted against normal load, F_n at Π_{dep} = 10 mN m^{-1}, expanded to show data at higher values of F_n for two different shear velocities, v_s. The solid and dashed lines are linear fits to different sections of the data, with the corresponding values of μ shown on the plot.

found in synovial joint lubrication in aqueous media ($\mu < 0.002$) [52,53], where a hydration lubrication mechanism [53,54] and supramolecular synergy between multiple components of the synovial fluid [55] leads to remarkably effective aqueous boundary lubrication. Such an observation is unprecedented for a neutral statistical copolymer in a non-polar solvent. However, for the LB films deposited at the two highest values of Π_{dep} = 15 and 20 mN m^{-1}, much higher friction was obtained, with $\mu \sim 0.14 - 0.15$ and $\mu \sim 0.2$ respectively, demonstrating a non-linear relationship between Π_{dep} and μ.

The shear behaviour at higher loads for Π_{dep} = 10 mN m^{-1} at different values of v_s was also investigated, as shown in Fig. 6**d**. The shear data at both values of v_s exhibit a clear transition to a higher value of μ above a certain normal load, F_n, indicating two different regimes of lubrication at low and high F_n, respectively. An abrupt increase in the COF at higher loads has been reported in the literature for polymer brushes [17] and adsorbed surfactant layers [56] in non-polar solvents. In both cases, this behaviour was attributed to an increased degree of interpenetration of the opposing layers at higher pressures and increased relaxation times of the polymer brushes or alkyl chains, which we believe is also responsible for the two-regime friction behaviour between the FOCP LB films reported here.

What accounts for the significant reduction in μ relative to physisorbed FOCP layers seen at Π_{dep} = 5 and 10 mN m^{-1}? As derived by Alexander [57] and de Gennes [46] for end-anchored polymer chains, interactions between adjacent layers of confined neutral polymers are dominated by the osmotic pressure, resulting from the entropic excluded volume effect which leads to a strong net repulsion between the adjacent monomers in a good solvent. The repulsive normal forces between the neutral FOCP LB films are of the same origin. We propose that the lateral compression of the LB films at the air–water interface prior to deposition increased the monomer packing density, compared to the physisorbed polymer layers (whose maximum packing density is limited by the steric

repulsion arising from previously adsorbed FOCP chains), reducing the extent of interpenetration between the opposing polymer layers when confined. With limited interpenetration, the rapid relaxation of the contacting polymer chains creates a fluid interface at the midplane that facilitates low friction sliding. The significant reduction in the COF from $\Pi_{dep} = 5$ mN m^{-1} to $\Pi_{dep} = 10$ mN m^{-1} would likely be explained by a greater monomer packing density in the latter case, leading to an optimal suppression of interpenetration and the resulting ultralow COF (μ = 0.002 – 0.011). From the corresponding normal force profiles measured in *n*-dodecane, the calculated values of $0.5D_{min}/L_0$ (the ratio of hard-wall thickness (for a single layer) to the unperturbed layer thickness) are 0.10 at $\Pi_{dep} = 5$ mN m^{-1} and 0.15 at $\Pi_{dep} = 10$ mN m^{-1}. This indicates that the FOCP LB films at $\Pi_{dep} = 10$ mN m^{-1} are less compressible and so provides evidence for a higher monomer packing density. The SLD values obtained from fitting the dry-film XRR data (Table 1) also support this hypothesis, with $\rho = 2.84$ and 3.34×10^{-6} Å^{-2} obtained at $\Pi_{dep} = 5$ and 10 mN m^{-1} respectively, suggesting a higher polymer volume fraction at $\Pi_{dep} = 10$ mN m^{-1}.

Comparable shear measurements were also performed between the dry LB films in air, prior to injection of the *n*-dodecane solvent; in all cases, a rigidly coupled shear response was seen, where the maximum applied shear amplitude could not overcome the static frictional force required to initiate sliding of the strongly adhered surfaces. This demonstrates that an important mechanistic role is played by the presence of the *n*-dodecane solvent confined between the adjacent polymer layers. When confined between hard, flat surfaces, the quasi-discrete layers formed by *n*-alkanes are known to exhibit solid-like properties below a critical number of layers, characterised by a viscosity increase by up to seven orders of magnitude and the ability to sustain a finite shear stress [38,50,58]. However, when confined between the FOCP LB films, which are molecularly rough and viscoelastically deformable, analogously to other examples of PFMs [9], the *n*-dodecane molecules cannot form well-ordered layers and solidify, allowing the solvent layer to retain its liquid-like dynamic properties and fluidity to enable sliding.

To investigate the significant difference in the lubrication behaviour between the LB films transferred at the lower pressures ($\Pi_{dep} = 5$ and 10 mN m^{-1}) and at the higher pressures ($\Pi_{dep} = 15$ and 20 mN m^{-1}), insights were obtained from two ancillary sets of SFA measurements. Firstly, prior to injection of the *n*-dodecane solvent between the surfaces, normal force profiles were obtained between the dry FOCP films prepared by LB deposition (**Fig. S1, Supplementary Information**). From the pull-off force, F_P/R, required to separate the two surfaces from adhesive contact, the surface energies, γ, of the dry FOCP LB films were calculated using the expression derived from Johnson-Kendall-Roberts (JKR) theory [51]: $\gamma = (-F_P/R)/(3\pi)$. The calculated values of $\gamma = 30.9$ ($\pm$2.3) mJ m^{-2} at $\Pi_{dep} = 5$ mN m^{-1}, $\gamma = 32.3$ ($\pm$4.0) mJ m^{-2} at $\Pi_{dep} =$ 10 mN m^{-1} and $\gamma = 32.6$ ($\pm$1.1) mJ m^{-2} at $\Pi_{dep} = 15$ mN m^{-1} indicate that the outermost layer of the deposited LB films presents a predominantly hydrophobic interface. The values are within or slightly higher than the literature range for a range of hydrocarbon solvents (γ = 22 – 28 mJ m^{-2}) [59], which can be attributed to interpenetration resulting from the roughness of the LB films. By comparison, a significantly higher value of $\gamma = 46.1$ ($\pm$1.5) mJ m^{-2} was obtained at $\Pi_{dep} = 20$ mN m^{-1}, which is too high to be explained by an increase in surface roughness alone; instead, it demonstrates a difference in the surface chemistry of the outermost layer in this case. This higher γ value also coincides with the attractive bridging interactions observed between the $\Pi_{dep} = 20$ mN m^{-1} LB films in *n*-dodecane upon retraction (cf. Fig. 5**b**). We attribute this increase in γ to an increased concentration of the polar-aromatic functional groups (FGs) of the FOCPs in the outermost layer of the LB films at the highest value of $\Pi_{dep} = 20$ mN m^{-1}. As all the LB films are otherwise chemically identical, the significant difference in γ must result from the greater degree of lateral packing of the FOCP chains at the air–water interface prior to their transfer to the mica surface.

Secondly, to gain further insight into the shear mechanism operating between the FOCP LB films at the different values of Π_{dep} we investigated the relationship between F_s and the shear velocity, v_s. Fig. 7**a** shows the v_s dependence of F_s at different values of Π_{dep}, recorded at relatively low applied loads of $F_n < 250$ μN, corresponding to $F_n/R < 25$ mN m^{-1} (where $R \sim 1$ cm) and $p < 19$ atm. At the lower values of $\Pi_{dep} = 5$ and 10 mN m^{-1}, F_s remained relatively constant over two orders of magnitude in v_s. This resembles solid–solid friction which is known to be very weakly dependent on sliding velocity as stated in Amontons' third law/Coulomb's law of friction [60]. If sliding is occurring at the polymer–polymer interfaces rather than at the polymer-substrate interfaces, the independence of F_s with respect to v_s is likely due to minimal interpenetration of the adjacent solvated polymer layers at the relatively low pressures used for these measurements. It means that the timescale associated with stretching and relaxation of the adjacent polymer chains would be sufficiently rapid relative to the applied sliding velocities ($v_s < 10$ μm s^{-1}) and so would not contribute appreciably to the energy barrier to the lateral sliding motion.

In contrast, for the films deposited at the higher surface pressures of $\Pi_{dep} = 15$ and 20 mN m^{-1}, F_s increased linearly with $\ln(v_s)$, markedly different from the behaviour exhibited at $\Pi_{dep} = 5$ and 10 mN m^{-1}. This is consistent with a rate-activated process, where a potential energy barrier must be overcome to initiate lateral motion/sliding. At a higher shear velocity, the probability of the potential energy barrier being overcome by the applied lateral force increases compared to if just random thermal fluctuations are operating, leading to an increase in shear stress and the prediction that shear force will increase as a function of v_s.

Several theoretical models based on the concept of activated slip exist, e.g. those of Eyring [61] and Shallamach [62]. Briscoe and Evans [23] applied Eyring's theory of liquid viscosity to boundary lubrication, leading to a relationship between shear force and velocity of the form $F_s = \left(\frac{A}{\Omega}\right)\Delta E + \left(\frac{Ak_BT}{\Omega}\right)\ln(v_s)$, where Ω is a characteristic activation volume, ΔE the activation energy that is required to be overcome to initiate sliding, A the contact area, and k_BT the thermal energy [63,64]. As shown in Fig. 7**a**, the data for $\Pi_{dep} = 15$ and 20 mN m^{-1} are consistent with this model, indicating that an activated slip mechanism is operating between the FOCP LB films.

The fitted activation energy is ΔE $(1.5-6) \times 10^{-20} J$ $(4-15) k_BT$. This can be related to the π–π interactions between the aminopheylaniline groups (cf. Fig. 5**d**) in the polar functional group, as well as the dipole interactions between the succinimide groups, the intermolecular forces for which would be in the order of $\sim 10\ k_BT$. Our SANS data (N. Taylor *et al.*, in preparation) show that the sticky functional groups drive polymer self-assembly in solution, and such associative behaviour of random copolymers bearing a similar succinimide group has also been recently reported [65]. We thus attribute the activation energy to the interactions between the functional groups of the polymer chains across the midplane. Polymer bridging in boundary lubrication in non-polar media has also been reported in the literature; for instance, Murdoch *et al.* postulated that these associative interactions were responsible for the boundary lubrication behaviour seen between adsorbed layers of a statistical nitroaniline-functionalized OCP between steel and silica surfaces in base-oil [65].

To verify that sliding was occurring at the polymer–polymer interaction zone rather than at the polymer-mica interfaces, we considered the interaction energy between a polymer FG and a mica surface. An enthalpy of adsorption of $\sim 29\ k_BT$ was obtained for the isolated FG at the mica-dodecane interface from a van't Hoff analysis of adsorption isotherms measured over a range of temperatures (N. Taylor *et al.*, in preparation). For sliding to occur at the polymer-mica interfaces, transient desorption of the FGs from the mica surface would have to occur, thus requiring a minimum activation energy of $\sim 29\ k_BT$. Additionally, this relates to only a single FG; each polymer chain will possess multiple FGs which would likely lead to multi-point adsorption to the mica surface, leading to much higher anchoring energy. The calculated range of $\Delta E \sim$ 4–15 k_BT is far lower than this, which infers that sliding is likely

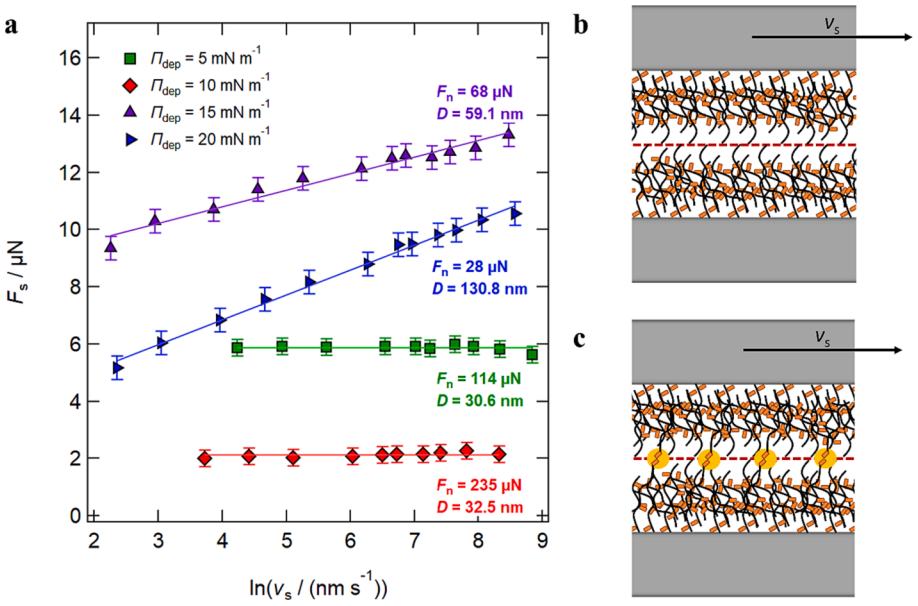

Fig. 7. (a) Shear force, F_s, plotted against the natural logarithm of sliding velocity, ln(v_s), measured at fixed normal load, F_n, for the four different values of Π_{dep}. The solid lines are linear fits and are included as guides to the eye. The linear increases in F_s as a function of ln(v_s) seen at Π_{dep} = 15 and 20 mN m^{-1} are indicative of a rate activated process, as discussed in the main text. (b) Proposed shear mechanism at Π_{dep} = 5 and 10 mN m^{-1}, where no significant polymer functional group bridging occurs between the adjacent layers. (c) Proposed shear mechanism at Π_{dep} = 20 mN m^{-1}, where significant polymer functional group bridging occurs at the slip-plane.

not occurring at the polymer-mica interfaces and so the shear stress must instead be dissipated within the interpenetration region between the adjacent polymer layers, where the energy barrier to lateral motion will be much lower.

The stress activated volume, Ω, in Eyring's model may be interpreted as the volume pervaded by the molecular moieties responsible for the activation energy. The fitted Ω values lie in the range 140–380 nm^3. We may estimate the size of the molecular moiety in the range of $\Omega^{1/3} \sim$ 5–7 nm. In fitting the surface force data (cf. Fig. 5**a**), we have obtained the inter-brush spacing, or effective de Gennes' blob size as s ∼ 4 – 5 nm, which is reasonably comparable to the calculated values of $\Omega^{1/3}$. We attribute Ω to the volume of a de Gennes' blob in the polymer layer structure, enclosing sticky joints between the functional groups.

We thus propose that the functionalised statistical polymer LB layer is characteristic of an *interfacial gel* with a thickness far exceeding that of a classic LB monolayer of polymers or surfactants, with the physical cross-linking points facilitated by the polymer FGs. The structure of the interfacial gel is characterised by de Gennes blobs, accounting for the polymer-brush-like behaviour observed from the surface force measurement – since the polymer brush structure is also characterised by the blobs. The solvent-swollen brush-like structure is robust against compression, capable of sustaining considerable osmotic pressure [66]. Upon shear, the relative weak physical cross-linking (∼10 k_BT interaction energy), identified as the molecular origin of the activation energy in Eyring's model, facilitates the relative ease of sliding and also reforming of the cross-linking joints, giving rise to a transient interfacial gel structure.

At Π_{dep} = 15 mN m^{-1}, where no significant bridging interactions were seen in the normal force profiles (**Fig. S2**, **SI**), we suggest that the observed activated-slip behaviour could arise from the roughness of the FOCP LB films. A similar rate-activated sliding behaviour was reported in SFB experiments between a hydrophilic mica surface and hydrophobic fluoropolymer surface in water, which was attributed to the deformation of asperities arising from the surface roughness of the polymer [67]. In this work, as revealed by XRR the surface roughness of the FOCP LB films increased significantly with Π_{dep}, which would increase the extent of interpenetration between the films even at lower confinement pressures and thus provide the energy barrier to lateral sliding required for a rate-activated process. Thus, we attribute the rate-activated behaviour observed at Π_{dep} = 15 and 20 mN m^{-1} to a combination of polymer layer interpenetration resulting from their increased surface roughness and the presence of FG-FG bridging interactions across the midplane, ultimately leading to their much higher values of μ.

4. Conclusions

Using the SFA, we have measured the normal and shear forces between Langmuir-Blodgett (LB) films formed by a statistical functionalised olefin copolymer (FOCP) in *n*-dodecane, as a function of the lateral packing density achieved at the air–water interface by varying the surface pressure, Π_{dep}, used for polymer LB deposition onto mica – the first such study for polymer LB films immersed in a non-polar solvent. The long-range interactions indicated that the solvent-swollen polymer layer thickness far-exceeded that expected of a classic LB monolayer, supported by complementary structural characterisation by XRR. The coefficient of friction, μ, measured between the confined LB films in *n*-dodecane varied non-linearly with respect to Π_{dep}, with ultralow synovial joint-esque lubrication (down to $\mu \sim 0.002$) achieved at Π_{dep} = 10 mN m^{-1} and much higher friction ($\mu > 0.1$) at Π_{dep} = 15 and 20 mN m^{-1}.

The drastically different friction behaviour was attributed to several factors relating to the molecular arrangement and interactions of the FOCPs across the midplane between the LB films. This was investigated by combining surface energy calculations between the dry LB films and probing the shear-velocity dependence of the shear force at low normal loads for all four values of Π_{dep}. A combination of polymer chain interpenetration resulting from increased surface roughness and the presence of FG-FG bridging interactions at the sliding interfaces are postulated as the mechanism behind the higher friction at larger values of Π_{dep}. We propose an interfacial gel structure for the LB-deposited statistical polymer layer, capable of transient structural transformation upon shear facilitated by the functional groups in the polymer architecture.

The results demonstrate the ability of LB deposition to act as a physical method to alter and tune desired tribological properties,

including the attainment of superlubricity ($\mu < 0.01$) which may aid in the development of new boundary lubrication strategies in oil. These results also point to the potential route to tailor the polymer architecture, e.g. the nature, density, and distribution of the functional groups, for controlling the interfacial structure and the nanotribological properties of confined macromolecular layers.

CRediT authorship contribution statement

Nicholas M. Taylor: Conceptualization, Investigation, Formal analysis, Data curation, Methodology, Writing – original draft, Writing – review & editing. **Georgia A. Pilkington:** Methodology, Writing – review & editing. **Tim Snow:** Software, Writing – review & editing. **Peter J. Dowding:** Conceptualization, Funding acquisition, Supervision. **Beatrice N. Cattoz:** Supervision. **Andrew D. Schwarz:** Supervision, Writing – review & editing. **Oier Bikondoa:** Investigation, Formal analysis, Writing – review & editing. **Brian Vincent:** Conceptualization, Funding acquisition, Supervision, Writing – review & editing. **Wuge H. Briscoe:** Conceptualization, Data curation, Funding acquisition, Supervision, Methodology, Project administration, Resources, Validation, Writing – original draft, Writing – review & editing.

Declaration of Competing Interest

The authors declare that they have no known competing financial interests or personal relationships that could have appeared to influence the work reported in this paper.

Data availability

Data will be made available on request.

Acknowledgements

N.M.T. gratefully acknowledges funding from Infineum UK Ltd, the EPSRC and the University of Bristol (The Everett Bequest Fund). W.H.B acknowledges funding from the EPSRC (EP/H034862/1) for the SFA experimental setup. Synchrotron XRR was performed at beamline BM28 at the ESRF (experiment number BM28-01-1193), a mid-range facility supported by the EPSRC, and we are grateful to all the beamline staff for their support. We are indebted to Anthony Strong (Infineum) for the synthesis of the polymers used in this work.

Appendix A. Supplementary material

Supplementary data to this article can be found online at https://doi.org/10.1016/j.jcis.2023.09.146.

References

[1] K. Holmberg, A. Erdemir, Influence of tribology on global energy consumption, costs and emissions, Friction 5 (3) (2017) 263–284, https://doi.org/10.1007/s40544-017-0183-5.
[2] K. Holmberg, P. Andersson, A. Erdemir, Global energy consumption due to friction in passenger cars, Tribol. Int. 47 (2012) 221–234, https://doi.org/10.1016/j.triboint.2011.11.022.
[3] R. Stribeck, Die wesentlichen Eigenschaften der Gleit- und Rollenlager (Characteristics of Plain and Roller Bearings), Zeit. des VDI 46 (1902).
[4] H. Spikes, Friction Modifier Additives, Tribol. Lett. 60 (2015) 1. DOI: ARTN 5 10.1007/s11249-015-0589-z.
[5] M. Smeeth, H. Spikes, S. Gunsel, Boundary film formation by viscosity index improvers, Tribol T 39 (3) (1996) 726–734, https://doi.org/10.1080/10402009608983590.
[6] G. Guangteng, M. Smeeth, P.M. Cann, H.A. Spikes, Measurement and modelling of boundary film properties of polymeric lubricant additives, Proc. Instit. Mech. Eng. 210 (1996) 1–15.
[7] M. Müller, K. Topolovec-Miklozic, A. Dardin, H.A. Spikes, The Design of Boundary Film-Forming PMA Viscosity Modifiers, Tribol T 49 (2) (2006) 225–232, https://doi.org/10.1080/05698190600614833.
[8] J. Fan, M. Müller, T. Stöhr, H.A. Spikes, Reduction of Friction by Functionalised Viscosity Index Improvers, Tribol. Lett. 28 (3) (2007) 287–298, https://doi.org/10.1007/s11249-007-9272-3.
[9] S. Yamada, A. Fujihara, S. Yusa, T. Tanabe, K. Kurihara, Low-Friction Adsorbed Layers of a Triblock Copolymer Additive in Oil-Based Lubrication, Langmuir 31 (44) (2015) 12140–12147, https://doi.org/10.1021/acs.langmuir.5b03620.
[10] S. Yamada, A. Fujihara, S.-I. Yusa, T. Tanabe, K. Kurihara, Confined film structure and friction properties of triblock copolymer additives in oil-based lubrication, Polym. J. 51 (1) (2018) 41–49, https://doi.org/10.1038/s41428-018-0114-y.
[11] S. Aoki, Y. Yamada, D. Fukada, A. Suzuki, M. Masuko, Verification of the advantages in friction-reducing performance of organic polymers having multiple adsorption sites, Tribol. Int. 59 (2013) 57–66, https://doi.org/10.1016/j.triboint.2012.06.001.
[12] N.F. Kossoko, F. Dubreuil, B. Thiébaut, M. Belin, C. Minfray, Diblock polymeric friction modifier (PFM) in the boundary regime: Tribological conditions leading to low friction, Tribol. Int. 163 (2021), 107186, https://doi.org/10.1016/j.triboint.2021.107186.
[13] T.A. Gmür, J. Mandal, J. Cayer-Barrioz, N.D. Spencer, Towards a Polymer-Brush-Based Friction Modifier for Oil, Tribol. Lett. 69 (4) (2021) 124, https://doi.org/10.1007/s11249-021-01496-w.
[14] C. Marques, J.F. Joanny, L. Leibler, Adsorption of Block Copolymers in Selective Solvents, Macromolecules 21 (4) (1988) 1051–1059, https://doi.org/10.1021/ma00182a035.
[15] S. Edmondson, V.L. Osborne, W.T.S. Huck, Polymer brushes via surface-initiated polymerizations, Chem. Soc. Rev. 33 (1) (2004) 14–22, https://doi.org/10.1039/B210143M.
[16] M. Ejaz, S. Yamamoto, K. Ohno, Y. Tsujii, T. Fukuda, Controlled Graft Polymerization of Methyl Methacrylate on Silicon Substrate by the Combined Use of the Langmuir−Blodgett and Atom Transfer Radical Polymerization Techniques, Macromolecules 31 (17) (1998) 5934–5936, https://doi.org/10.1021/ma980240n.
[17] J. Klein, E. Kumacheva, D. Mahalu, D. Perahia, L.J. Fetters, Reduction of Frictional Forces between Solid-Surfaces Bearing Polymer Brushes, Nature 370 (6491) (1994) 634–636, https://doi.org/10.1038/370634a0.
[18] R.M. Bielecki, E.M. Benetti, D. Kumar, N.D. Spencer, Lubrication with Oil-Compatible Polymer Brushes, Tribol. Lett. 45 (3) (2012) 477–487, https://doi.org/10.1007/s11249-011-9903-6.
[19] R.M. Bielecki, P. Doll, N.D. Spencer, Ultrathin, Oil-Compatible, Lubricious Polymer Coatings: A Comparison of Grafting-To and Grafting-From Strategies, Tribol. Lett. 49 (1) (2013) 273–280, https://doi.org/10.1007/s11249-012-0065-y.
[20] S. Watson, S. Dennington, L. Wang, M. Nie, S. Hinder, K. Stokes, Polymer brush lubrication of the silicon nitride–steel contact: a colloidal force microscopy study, RSC Adv. 7 (68) (2017) 42667–42676, https://doi.org/10.1039/C7RA08897C.
[21] K.B. Blodgett, Films built by depositing successive monomolecular layers on a solid surface, J. Am. Chem. Soc. 57 (1) (1935) 1007–1022, https://doi.org/10.1021/ja01309a011.
[22] B.J. Briscoe, D.C.B. Evans, D. Tabor, The influence of contact pressure and saponification on the sliding behavior of stearic acid monolayers, J. Colloid Interface Sci. 61 (1) (1977) 9–13, https://doi.org/10.1016/0021-9797(77)90411-8.
[23] B.J. Briscoe, D.C.B. Evans, The Shear Properties of Langmuir-Blodgett Layers, Proc. Roy Soc. Lond. a Mat. 380 (1779) (1982) 389, https://doi.org/10.1098/rspa.1982.0048.
[24] T. Ginnai, A. Harrington, V. Rodov, M. Matsuno, K. Saito, Langmuir-Blodgett films as lubricating layers for enhancing the useful life of high density hard disks, Thin Solid Films 180 (1) (1989) 277–286, https://doi.org/10.1016/0040-6090(89)90084-9.
[25] T. Miyashita, X.-D. Li, A. Aoki, Frictional Properties of Polymer Langmuir-Blodgett Film for Poly(N-dodecylacrylamide), Polym. J. 27 (11) (1995) 1154–1156, https://doi.org/10.1295/polymj.27.1154.
[26] F. Fan, X.-D. Li, T. Miyashita, Frictional properties of poly(N-polyfluoroalkylacrylamides) Langmuir-Blodgett films, Thin Solid Films 348 (1) (1999) 238–241, https://doi.org/10.1016/S0040-6090(99)00043-7.
[27] M. Aminuzzaman, Y. Kado, M. Mitsuishi, T. Miyashita, Frictional properties of an immobilized fluorinated polymer nanosheet, Thin Solid Films 516 (1) (2007) 67–71, https://doi.org/10.1016/j.tsf.2007.05.025.
[28] A.B. Gutierrez, D W; J.E. Johnston, Ethylene copolymer viscosity index improver-dispersant additive useful in oil compositions. United States 1986.
[29] B. Sironi, T. Snow, C. Redeker, A. Slastanova, O. Bikondoa, T. Arnold, J. Klein, W. H. Briscoe, Structure of lipid multilayers via drop casting of aqueous liposome dispersions, Soft Matter 12 (17) (2016) 3877–3887, https://doi.org/10.1039/c6sm00369a.
[30] W.H. Briscoe, M. Chen, I.E. Dunlop, J. Klein, J. Penfold, R.M. Jacobs, Applying grazing incidence X-ray reflectometry (XRR) to characterising nanofilms on mica, J. Colloid Interface Sci. 306 (2) (2007) 459–463, https://doi.org/10.1016/j.jcis.2006.10.031.
[31] W.H. Briscoe, F. Speranza, P.X. Li, O. Konovalov, L. Bouchenoire, J. van Stam, J. Klein, R.M.J. Jacobs, R.K. Thomas, Synchrotron XRR study of soft nanofilms at the mica-water interface, Soft Matter 8 (18) (2012) 5055–5068, https://doi.org/10.1039/c2sm07179g.
[32] C. Redeker, W.H. Briscoe, Interactions between Mutant Bacterial Lipopolysaccharide (LPS-Ra) Surface Layers: Surface Vesicles, Membrane Fusion, and Effect of Ca2+and Temperature, Langmuir 35 (48) (2019) 15739–15750, https://doi.org/10.1021/acs.langmuir.9b02609.

[33] W.H. Briscoe, S. Titmuss, F. Tiberg, R.K. Thomas, D.J. McGillivray, J. Klein, Boundary lubrication under water, Nature 444 (7116) (2006) 191–194, https://doi.org/10.1038/nature05196.
[34] M. Zhang, J. Duhamel, M. van Duin, P. Meessen, Characterization by Fluorescence of the Distribution of Maleic Anhydride Grafted onto Ethylene−Propylene Copolymers, Macromolecules 37 (5) (2004) 1877–1890, https://doi.org/10.1021/ma035906e.
[35] L. Wilhelmy, Ueber die Abhängigkeit der Capillaritäts-Constanten des Alkohols von Substanz und Gestalt des benetzten festen Körpers, Annalen der Physik 195 (6) (1863) 177–217, https://doi.org/10.1002/andp.18631950602 (acccessed 2020/04/22).
[36] L.A. Tsarkova, P.V. Protsenko, J. Klein, Interactions between Langmuir-Blodgett polymer monolayers studied with the surface force apparatus, Colloid J+ 66 (1) (2004) 84–94, https://doi.org/10.1023/B:Coll.0000015062.45958.90.
[37] L.G. Parratt, Surface Studies of Solids by Total Reflection of X-Rays, Phys. Rev. 95 (2) (1954) 359–369, https://doi.org/10.1103/PhysRev.95.359.
[38] J. Klein, E. Kumacheva, Simple liquids confined to molecularly thin layers. I. Confinement-induced liquid-to-solid phase transitions, J. Chem. Phys. 108 (16) (1998) 6996–7009, https://doi.org/10.1063/1.476114.
[39] J.N. Israelachvili, Thin Film Studies Using Multiple-Beam Interferometry, J. Colloid Interface Sci. 44 (1973) 259–272.
[40] B.V. Derjaguin, Untersuchungen über die Reibung und Adhäsion, IV. *Kolloid-Zeitschrift* 69 (1934) 155–164.
[41] H. Kiessig, Interferenz von Röntgenstrahlen an dünnen Schichten, Annalen der Physik 10 (1931) 769–788.
[42] T.J. Su, D.A. Styrkas, R.K. Thomas, F.L. Baines, N.C. Billingham, S.P. Armes, Neutron and X-ray Reflectivity Studies of Water-Soluble Block and Statistical Copolymers Adsorbed at the Air−Water Interface, Macromolecules 29 (21) (1996) 6892–6900, https://doi.org/10.1021/ma960218z.
[43] J. Kim, J.C. Kim, M.D. Phan, H. Kim, K. Shin, M. Ree, Self-assembling characteristics of amphiphilic zwitterionic brush random copolymers at the air–water interface, RSC Adv. 7 (20) (2017) 11813–11820, https://doi.org/10.1039/C6RA28828F.
[44] H.K. Christenson, D.W.R. Gruen, R.G. Horn, J.N. Israelachvili, Structuring in liquid alkanes between solid surfaces: Force measurements and mean-field theory, J. Chem. Phys. 87 (3) (1987) 1834–1841, https://doi.org/10.1063/1.453196 (acccessed 2020/07/02).
[45] A.M. Smith, J.E. Hallett, S. Perkin, Solidification and superlubricity with molecular alkane films, Proc. Natl. Acad. Sci. 116 (51) (2019) 25418, https://doi.org/10.1073/pnas.1910599116.
[46] P.G. De Gennes, Scaling Concepts in Polymer Physics, Cornell University Press, 1979.
[47] P.J. Flory, Principles of Polymer Chemistry, Cornell University Press, 1953.
[48] M. Zhang, J. Duhamel, Study of maleated ethylene–propylene copolymers by fluorescence: Evidence for succinimide induced polar associations in an apolar solvent, Eur. Polym. J. 44 (9) (2008) 3005–3014, https://doi.org/10.1016/j.eurpolymj.2008.06.017.
[49] L.M. Qian, G. Luengo, E. Perez, Thermally activated lubrication with alkanes: The effect of chain length, Europhys. Lett. 61 (2) (2003) 268–274, https://doi.org/10.1209/epl/i2003-00228-6.
[50] M.L. Gee, P.M. McGuiggan, J.N. Israelachvili, A.M. Homola, Liquid to solidlike transitions of molecularly thin films under shear, J. Chem. Phys. 93 (3) (1990) 1895–1906, https://doi.org/10.1063/1.459067 (acccessed 2020/07/02).
[51] K.L. Johnson, Contact Mechanics, Cambridge University Press, 2004.
[52] H. Forster, J. Fisher, The Influence of Loading Time and Lubricant on the Friction of Articular Cartilage, Proc. Inst. Mech. Eng. [H] 210 (2) (1996) 109–119, https://doi.org/10.1243/PIME_PROC_1996_210_399_02 (acccessed 2019/04/12).
[53] W.H. Briscoe, Aqueous boundary lubrication: Molecular mechanisms, design strategy, and terra incognita, Curr. Opin. Colloid Interface Sci. 27 (2017) 1–8, https://doi.org/10.1016/j.cocis.2016.09.002.
[54] U. Raviv, J. Klein, Fluidity of Bound Hydration Layers, Science 297 (5586) (2002) 1540, https://doi.org/10.1126/science.1074481.
[55] J. Seror, L. Zhu, R. Goldberg, A.J. Day, J. Klein, Supramolecular synergy in the boundary lubrication of synovial joints, Nat. Commun. 6 (2015) 6497, Article. DOI: 10.1038/ncomms7497.
[56] S.M. Lundgren, M. Ruths, K. Danerlov, K. Persson, Effects of unsaturation on film structure and friction of fatty acids in a model base oil, J. Colloid Interface Sci. 326 (2) (2008) 530–536, https://doi.org/10.1016/j.jcis.2008.05.068.
[57] S. Alexander, Adsorption of chain molecules with a polar head a scaling description, J. Phys. France 38 (8) (1977) 983–987, https://doi.org/10.1051/jphys:01977003808098300.
[58] E. Kumacheva, J. Klein, Simple liquids confined to molecularly thin layers. II. Shear and frictional behavior of solidified films, J. Chem. Phys. 108 (16) (1998) 7010–7022. DOI: 10.1063/1.476115 (acccessed 2020/07/02).
[59] J.N. Israelachvili, Intermolecular and Surface Forces, Academic Press, 2011.
[60] F.P. Bowden, D. Tabor, The Friction and Lubrication of Solids, Clarendon Press, 1971.
[61] H. Eyring, Viscosity, Plasticity, and Diffusion as Examples of Absolute Reaction Rates, J. Chem. Phys. 4 (4) (1936) 283–291, https://doi.org/10.1063/1.1749836 (acccessed 2019/07/23).
[62] A. Schallamach, The Velocity and Temperature Dependence of Rubber Friction, Proc. Phys. Soc.. Section B 66 (5) (1953) 386-392. DOI: 10.1088/0370-1301/66/5/306.
[63] L. Ma, A. Gaisinskaya-Kipnis, N. Kampf, J. Klein, Origins of hydration lubrication, Nat. Commun. 6 (1) (2015) 6060, https://doi.org/10.1038/ncomms7060.
[64] A. Gaisinskaya-Kipnis, L. Ma, N. Kampf, J. Klein, Frictional Dissipation Pathways Mediated by Hydrated Alkali Metal Ions, Langmuir 32 (19) (2016) 4755–4764, https://doi.org/10.1021/acs.langmuir.6b00707.
[65] T.J. Murdoch, E. Pashkovski, R. Patterson, R.W. Carpick, D. Lee, Sticky but Slick: Reducing Friction Using Associative and Nonassociative Polymer Lubricant Additives, ACS Appl. Polym. Mater. 2 (9) (2020) 4062–4070, https://doi.org/10.1021/acsapm.0c00687.
[66] M. Chen, W.H. Briscoe, S.P. Armes, J. Klein, Lubrication at physiological pressures by polyzwitterionic brushes, Science 323 (5922) (2009) 1698–1701, https://doi.org/10.1126/science.1169399 From NLM Medline.
[67] I. Rosenhek-Goldian, N. Kampf, J. Klein, Trapped Aqueous Films Lubricate Highly Hydrophobic Surfaces, ACS Nano 12 (10) (2018) 10075–10083, https://doi.org/10.1021/acsnano.8b04735.